Journal of Engineering Science and Technology Review 17 (2) (2024) 182 - 189

Research Article

JOURNAL OF
Engineering Science and Technology Review

www.jestr.org

Hysteresis current control of Vienna Rectifier for Electric Vehicle Charging Systems

Bharaneedharan Balasundaram and Suresh Panchanathan*

Department of Electrical and Electronics Engineering, SRM Institute of Science and Technology, Kattankulathur,nChennai, Tamil Nadu – 603203, India

Received 22 January 2024; Accepted 19 April 2024

Abstract

The energy savings, pollution reduction, and environmental protection offered by electric vehicles are superior to those of fuel-powered vehicles. The availability of electric vehicle charging infrastructure is significantly less in India, which is becoming an impediment to the widespread use of electric vehicles due to the range and charging anxieties among the people. Modern power electronic converters play a vital role in electric vehicle charging applications. The output obtained from the converters is harmonic and distorted. The output voltage has to be enhanced to make the PI controller a hysteresis current controller for charging electric cars, and the ripples can be minimized using a Vienna rectifier. There is no harmonic content in the Vienna rectifier at the grid side, which improves the power factor and efficiency. A Vienna rectifier lowers the amount of power that switches use and increases the power density of the system for superior DC charging of electric vehicles. The THD value of the input current can be suppressed to a level below 5%. with the proposed hysteresis current controller and Vienna rectifier. The Vienna rectifier control simulation model is built in MATLAB or Simulink.

Keywords: Vienna Rectifier, Hysteresis Current Controller, Electric Vehicles, Charging Stations, Total Harmonic Distortion.

1. Introduction

To alleviate consumer fear and promote the adoption of electric vehicles, it is now clear that a comprehensive network of charging stations is necessary. Regulators establish charging standards to ensure uniformity in electric vehicle chargers [1]. Methods like CHADEMO have become popular and are generally well-received. Several standards, including BHARAT DC 001 for direct current charging and Bharat AC 001 for alternating current charging, have been produced by the Indian government as part of its effort to uniformly regulate EV chargers[2], [3]. Research on EV charging standards has been detailed in several publications[4–6]. From a technical and environmental perspective, this article analyses WPT technology as it pertains to electric vehicle applications [7]. The article [8] discusses several topologies for various EV charging types. The architecture of the rapid charging station and the structures of the power converters used in the AC to DC and DC to DC power stages are explained in[9]. For electric vehicle (EV) adoption to accelerate, it is critical to study the EV charging infrastructure. Present and future trends in the global electric car market are explored in this article [10]. When charging an electric vehicle, it is necessary to provide the battery with electricity at the correct voltage and current levels, which are dependent on the battery's specifications. Find out more about the power ratings, norms, and infrastructure of electric vehicle charging in India. Power outputs ranging from 50 kW to 200 kW are specified by IS-17017-Part-23 for DC charging stations. Large vehicles, like buses, must adhere to stringent power charging regulations. To meet the needs of light electric vehicles with a DC power output of less than 7 kW, the Bureau of Indian Standards (BIS) has just completed IS-17017-Part-25 [11].

Depending on the level of power, electric vehicles can be charged up to 22 kW for ordinary charging and up to 200 kW for adequate charging. Despite the widespread availability of EVSEs with power ratings of up to 500 kW, these are mainly designed for use with large vehicles such as trucks and buses. Significant applications, including electric vehicle charging stations, welding power sources, and aircraft use [12–16], have extensively used the Vienna rectifier. In [17] article reviews various bidirectional converter topologies used in the V2G system. Industry and academics have focused on the Vienna rectifier topology due to its high performance, minimal losses, and simplified control technique [18]. For medium- and high-power applications, the Vienna rectifier offers the essential properties of lowering input current THD and increasing power factor at AC mains electricity sources. But when switching activities with large frequency ranges and an increase in power density, the dependability of power converters decreases, and malfunctions harm system performance [19]. Due to temperature changes, overloads, and improper gate driving signals, the Vienna rectifier in three phases experiences a shock of high-frequency voltage. while charging electric vehicles [20–22].

The Vienna rectifier is preferred for lowering harmonic distortion and enhancing the power factor. Vienna rectifier switching losses are minimal since the switches are not under a lot of voltage stress. [23-24]. With only one active switch required for each phase, the Vienna rectifier is both more convenient and dependable. Power factor adjustment is determined by the boost inductor located at the input of this converter, which is effectively a pulse width modulation converter [25]. When the switch is activated, the energy previously stored in the inductor while the switch was inactive is transmitted to the load via the diodes. This article [26] discusses a voltage-oriented controller with a Vienna rectifier for high-power applications.

*E-mail address: suresh.au95@gmail.com
ISSN: 1791-2377
doi:10.25103/jestr.172.19

Innovative power electronics and semiconducting devices are incorporated into electrical systems. To achieve unity power factor and limit harmonics, control devices such as the proportional integral controller, hysteresis current controller, and proportional controller are utilized [27]. The controllers can reduce and manage the switching frequency of the converter, resulting in harmonic content that is well-defined [28].

The most complicated approach is used by predictive controllers, which necessitate knowledge of load parameters and the use of high-level hardware. Simple, stable, error-free tracking, quick transient response, and intrinsically resilient to load factors are all characteristics of hysteresis current controllers [29]. The hysteresis control mechanism is engineered to align the inductor current with the rectified AC line voltage's form. This control has many benefits, such as not requiring a compensation ramp, transforming a voltage source to a rapid-current source, having a very simple-to-design inductor, functioning at a rapid switching, minimally distorted input current waveforms, and a constant load. The switching pulse is generated using the hysteresis current control approach [30–34]. Table 1 shows the different charging standards for EV charging.

Table 1. IS, IEC, SAE, CHADEMO, BHARATH standards: power, current AC, and DCCharging levels.

No	Charging Standards	Charging Power	Power Level	Types of Supply	EV Vehicles	Charging Current
1	IS-17017-PART-25	Average power charging	Up to7 kW	AC & DC	EV-2,3-wheelers, and EV cars (up to 1 ton)	80A
2	IS-17017-PART-22		7 to 22kW	AC & DC		80A
3	IS-17017-PART-22	Large power charging	22 to 50 kW	DC	EV-4 wheelers, LCVs, and MCVs (1 to 6 tons)	200A
4	IS-17017-PART-23		50 to 200 kW	DC		400A
5	IEC STANDARDS IEC61851-22 IEC 61851-23	Large power charging	100-200kW	DC	EVs, LCVs, and MCVs in the 1–6 tons)	400A
6	SAE SAE J2293	Large power charging	40kW	DC	EV-cars, LCVs, and MCVs (1 to 6 tons)	80A
			90 kW	DC	EV-4 wheelers, LCVs, and MCVs (1 to 6 tons)	200A
			240 kW	DC	EV-cars, MCVs (1 to 12 tons)	400A
7	IEC 62196-3 IEEE 2030.1.1 CHADEMO	Large power charging	400 kW	DC	EV-cars, MCVs (1 to 18 tons)	400A
8	BHARAT EV IEC 60309 IEC61851-1	Average power charging range	3.3-15 kW	DC	EV-2, 3-wheelers, and EV cars (up to 1 ton)	200A

2. Operating Principle of Vienna Rectifier

One common arrangement for PFC correction of the rectifier circuit is a Vienna rectifier. A three-phase diode bridge rectifier is the components that make up the rectifier. The circuit topology is shown in Fig. 1. The rectifier is made up of three switches such as Sa, Sb, and Sc. Additionally, it contains a load resistance R, DC load side capacitors C1 and C2, six diodes D1-D6, and an inductor La, Lb, and Lc. Closing the switch causes the DC capacitor to discharge and the inductor to charge. Turning off the switch discharges the boost inductor. Its structure and operating principle are comparable to those of a boost circuit. The switch comprises a MOSFET switch; it minimizes the voltage stress. The circuit contains two diodes that lower the losses in the diodes, and the switch's rating has decreased; this results in a decrease in the device's cost, and count and an increase in efficiency. There is a voltage stress of Vdc/2 on all semiconductor switches and diodes.

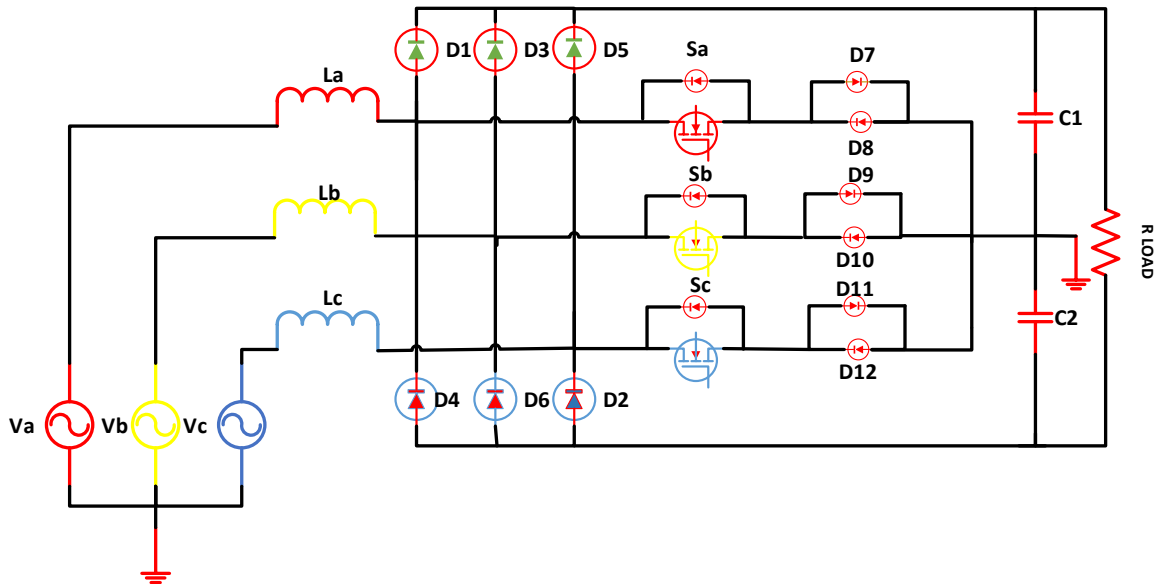

Fig. 1. Topology of the three-phase three-level Vienna rectifier.

The voltage for all phases can be computed using the Vienna rectifier's three switches in conjunction with the phase current's polarity and the (ON\OFF) state. Assuming a constant VDC output voltage, there are three possible amounts of input current: VDC/2, 0, and -VDC/2. By focusing on phase, A, we can understand how the Vienna rectifier works; the remaining phases work in a manner identical to phase A.

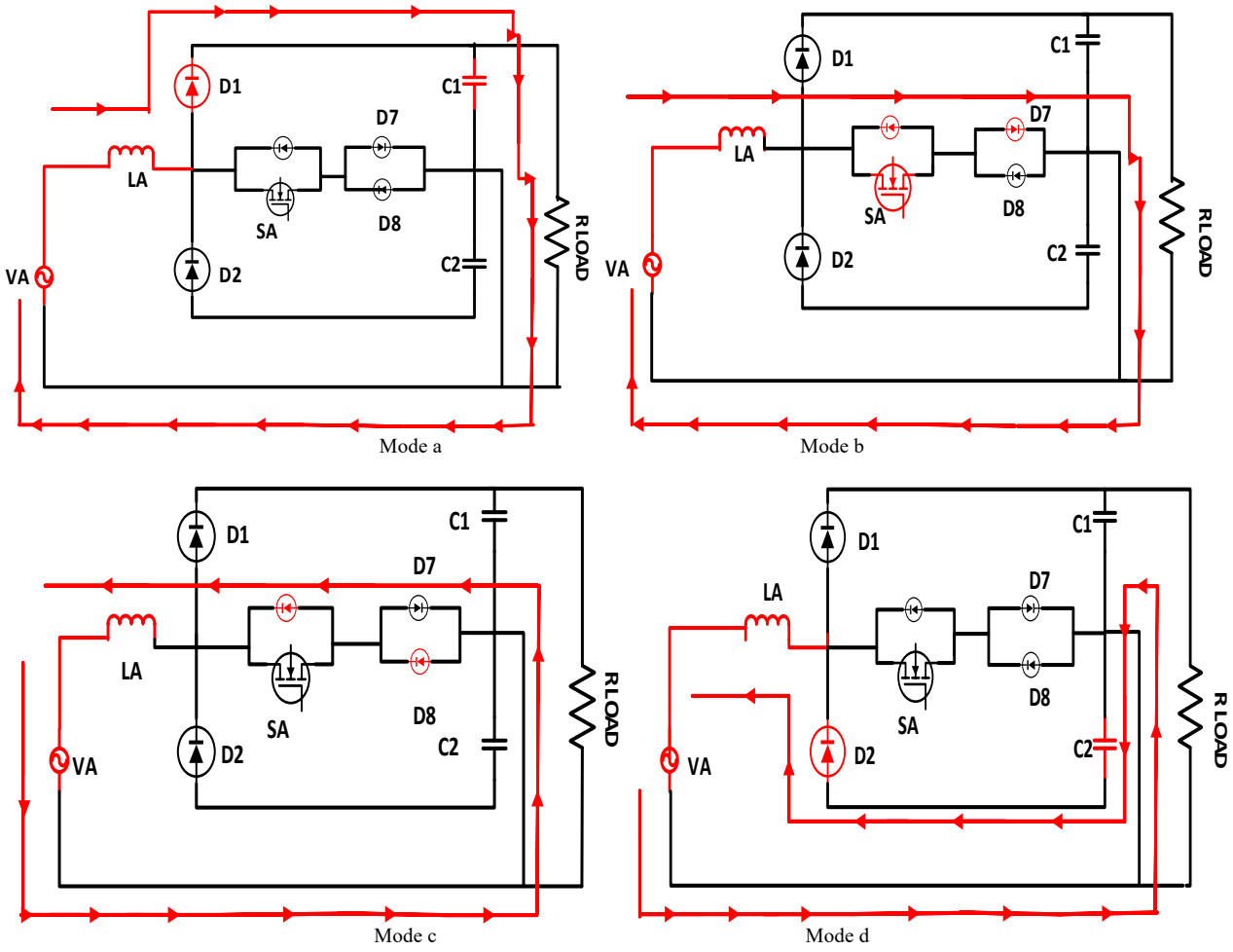

Fig. 2 (a-d) Modes of operation for Vienna rectifier

Mode 1[Fig. 2(a)]: As demonstrated in Fig. 2, when the switch SA is turned off and there is a positive phase current the current charges the capacitor C1 through the freewheeling diode D1 and then returns to neutral. The flow of current for mode-I is Va, La, D1, and C1. The power loss is lower because only one diode is involved.

Mode 2[Fig. 2(b)]: When turned on, the current flows through neutral, the switch SA, and diode D8, taking the low-resistance route. The flow of current for mode-2 is Va, La, SA, and D7. Power loss is lower in this cycle as well because diode D8 is the only component providing resistance.

Mode 3[Fig. 2(c)]: When turned on, diode D8 completes a full circuit by reversing the normal flow of current that is, from neutral to the source. When the current is less than zero. The flow of current for mode-3 is Va, C2, D8, and La, Similarly, low loss is achieved because the loss happens solely in the diode.

Mode 4[Fig. 2(d)]: With the switch, SA turned off, current flows from the neutral via freewheeling diode D2 to the source. The flow of current for mode-4 is C2, D2, La, and Va, respectively. when the current level is lower than zero.

For example, a range of 120° to 180° is used. Table 2 displays the potential at the rectifier's input end for eight distinct switch configurations.

Table 2. Output voltage under a range of 120° to 180° eight different switch states

S.NO	SA	SB	SC	VAO	VBO	VCO
I	0	0	0	$V_{dc}/2$	$V_{dc}/2$	$-V_{dc}/2$
II	0	0	1	$V_{dc}/2$	$V_{dc}/2$	0
III	0	1	0	$V_{dc}/2$	0	$-V_{dc}/2$
IV	0	1	1	$V_{dc}/2$	0	0
V	1	0	0	0	$V_{dc}/2$	$-V_{dc}/2$
VI	1	0	1	0	$V_{dc}/2$	0
VII	1	1	0	0	0	$-V_{dc}/2$
VIII	1	1	1	0	0	0

Diode DF average & RMS current:

$$I_{DFavg} = \left(\frac{1}{2\sqrt{3}m}\right)\hat{I}_N X\sqrt{2} \quad (1)$$

$$I_{DFavg} = \left(\frac{1}{2\sqrt{3}X1.11346}\right)12.698\,X\sqrt{2}$$

$$I_{DFavg} = 4.655\,A$$

$$I_{DFrms} = \sqrt{\left(\left(\frac{4}{3\sqrt{3\pi}}X\frac{1}{m}\right)\right)}.\hat{I}_N X\sqrt{2} \quad (2)$$

$$I_{DFrms} = \sqrt{\left(\left(\frac{4}{3\sqrt{3\pi}}X\frac{1}{1.11346}\right)\right)}12.698\,X\sqrt{2}$$

I_{DFrms}=8.426 A

Switch S average & RMS current:

$$I_{Savg}=\left[\frac{2}{\pi}-\frac{1}{\sqrt{3m}}\right]\hat{I}_N X\sqrt{2} \quad (3)$$

$$I_{Savg}=\left[\frac{2}{\pi}-\frac{1}{\sqrt{3}X1.1134}\right]12.698X\sqrt{2}$$

$$I_{Savg}=2.1256A$$

$$I_{Srms}=\sqrt{\left(\frac{1}{2}-\frac{8}{3\sqrt{3}}.\frac{1}{m}\right)}.\hat{I}_N X\sqrt{2} \quad (4)$$

$$I_{Srms}=\sqrt{\left(\frac{1}{2}-\frac{8}{3\sqrt{3}}.\frac{1}{1.1134}\right)}12.698X\sqrt{2}$$

$$I_{Srms}=16.864A$$

However, the MOSFETs in switch S are connected back-to-back. MOSFETs of S+ and diodes of S- conduct at the positive half cycle, while MOSFETs of the S- and diodes of S+ exhibit conductivity in the negative half cycle. Therefore, the equations listed below determine the current in a MOSFET or diode of type S.

$$I_{T\,avg}=\sqrt{\left(\frac{1}{\pi}-\frac{1}{2\sqrt{3m}}\right)}.\hat{I}_N X\sqrt{2} \quad (5)$$

$$I_{T\,avg}=\sqrt{\left(\frac{1}{\pi}-\frac{1}{2\sqrt{3}X1.1134}\right)}12.698X\sqrt{2}$$

$$I_{T\,avg}=4.369A$$

$$I_{Trms}=\sqrt{\left(\frac{1}{4}-\frac{4}{3\sqrt{3}\pi}\frac{1}{M}\right)}\hat{I_N}X\sqrt{2} \quad (6)$$

$$I_{T\,rms}=\sqrt{\left(\frac{1}{4}-\frac{4}{3\sqrt{3\pi}}.\frac{1}{1.1134}\right)}12.698X\sqrt{2}$$

$$I_{T\,rms}=11.929A$$

A. Calculating Losses and Efficiency

For Diodes

(i) Conduction losses = $I_{avg}\,X\,V_F$ = 2.1256 X 1.5 (7)

Conduction losses=3.1884W

The data sheet provides information on V_f, which represents the voltage drop across the diode in the direction at the specified I_{ave}. The range of V_f values is (0.6v to 1.6v).

(ii) Switching loss = $\frac{1}{2}CV^2$f (8)

The variables in the equation are C, which signifies the junction's capacitance, V, which represents the blocking voltage, and f, which represents the switching frequency.

For MOSFET's

(i) Conduction loss = $I^2_{rms}\,X\,R_{DS_{ON}}$ = $(11.929)^2$ X 0.38 (9)

Conduction losses=54.07 W

Where $R_{DS_{ON}}$ is the resistance between the source and drain terminal.

(ii) Switching loss

Turn-on loss= $\frac{1}{2}VI_{rms}t_r f_{sw}$ (10)

Turn-off loss= $\frac{1}{2}VI_{rms}t_f f_{sw}$ (11)

The switching frequency is denoted by fsw, the rise time is represented by tr, and the fall time is shown by t_f.

3. Design of Modified Vienna Rectifier

A. Inductor Selection

A series of inductors connected to the three-phase input voltage dampens input current waves in a Vienna rectifier. Most conversion operations use the inductor value from the data sheets. However, a tremendous amount of voltage conversion still takes place. Consequently, the following equation is used to find the inductor value for this voltage conversion range.

B. Inductor value of Vienna rectifier,

Inductor, La = Lb = Lc = L,

$$L=\frac{V_{in}X(V_{out}-V_{in})}{\Delta_{IL}\,X\,f_s\,XV_{out}} \quad (12)$$

$$L=\frac{420X(810-420)}{3.29X20000\,X810}$$

$$L=0.3H$$

C. Capacitor selection

To determine the value of the capacitor, use the following equation. Additionally, the capacitor lessens voltage ripple and input/output current fluctuations.

Capacitor, Ca = Cb = Cc = C,

$$C=\frac{I_{out}X\Delta}{f_s\times\Delta Vc} \quad (13)$$

$$C=\frac{19.45X0.48148}{20000\times162}$$

$$C=7982F$$

4. Design of a Controller for Modified Vienna Rectifier

This section explains the controller design for the upgraded Vienna rectifier. The Three-phase Vienna rectifier with hysteresis current controller is shown in Fig. 3. With the summer function, the proportional-integral (PI) controller adds the reference and output voltages. The proportional integral controller (PI) regulates the DC output voltage. The standard approach to control uses a PI controller to keep an eye on the current loop. On the power grid, you might find harmonic current because PI control isn't perfect at ensuring a perfect current tracking reference signal. Hence, the hysteresis current controller greatly improves tracking while also decreasing periodic disturbances. Indeed, hysteresis-current control provides a more precise method of blocking periodic disturbance signals and more accurate steady-state outcomes. A longer time is still required for the dynamic process, and the power frequency period is still used as a stage in the correction process. To successfully eliminate harmonic voltage interference, this paper employs a control scheme that combines PI controllers with hysteresis current in parallel. This enhances tracking precision while preserving the PI control's quick reaction channel.

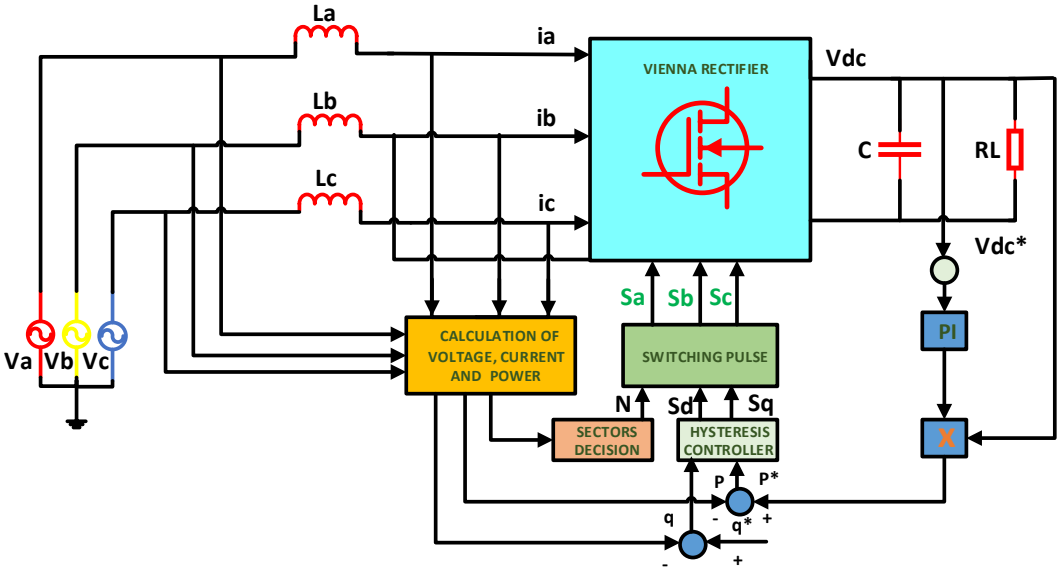

Fig. 3. Three-phase Vienna rectifier with hysteresis current controller.

5. PI Controller

Maintaining a constant voltage is controlled by the magnitude inaccuracy in DC voltage. Fig. 4 shows the corresponding DC voltage regulation loop schematic, which is useful when thinking about the RC circuit on the output side. This current at output is

$$i = k_1 \Delta V_{dc} + \int k_2 \Delta V_{dc} dt \tag{14}$$

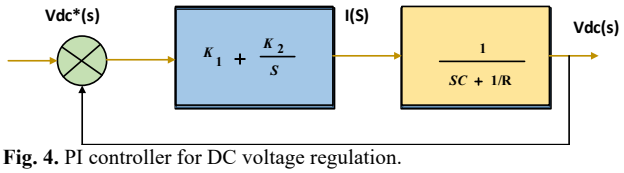

Fig. 4. PI controller for DC voltage regulation.

The integral gain of the loop is denoted by k2, whereas the proportional gain is k1. A transfer function that is closed-loop is defined as

$$\frac{V_{dc}(S)}{V_{dc}^{*}(S)} = \frac{k_1 R(s + \frac{k_2}{k_1})}{s^2 + 2\xi\omega_n s + \omega_n^2)} \tag{15}$$

Where $k_1 = 2\xi\omega_n C - \frac{1}{R}$ and $k_2 = \omega_n^2 C$ (16)

6. Modified Hysteresis Controller

The most significant issue with traditional fixed-hysteresis band current management is the generation of excessive current ripple caused by the variation in modulation frequency within a band. The output filter design was challenged by this modulation frequency change. As a result of the relatively consistent switching frequency, it also allows for an output filter design that is easier to work with. Conversely, this hysteresis band current control can lessen switching losses.

The Hysteresis Current Controller has some drawbacks that the PI Controller helps to fix. The combination's non-static PWM frequency is the controller's main drawback since it causes less-than-ideal harmonics. Since it uses PWM, an instantaneous feedback control method, the Modified Hysteresis Controller was selected. This controller's command current follows the actual current in real time, as long as it stays within a certain hysteresis band. Integral gain is used to eliminate steady-state errors, while proportional gain improves the rise time. With the help of two control loops, we can maintain a steady output voltage and bring the power factor to unity.

If the voltage at the DC output is measured in a voltage-control loop, then the error can be estimated. The control loop for the DC output voltage uses feedback to keep the capacitor voltage at a reference value. A PI controller, also known as a voltage compensator or integrator, is used to control the DC output error. The current control loop takes the PI controller's output and adjusts the duty ratio to preserve the DC output voltage constant.

Similarly, rectifiers utilized in applications with high levels of performance have grown in significance due to the

necessity of current control approaches. These converters must respond quickly and accurately in these applications. This is where the present control loop employs the hysteresis control technique.

Here are the outcomes that the controller has accomplished:

(i) On the main side, we get a power factor value that is one or very near to one.
(iii). The alternating current mains can only produce line currents with a sinusoidal waveform.
(iii). The system's neutral point is balanced, and the DC output voltage is maintained constant.

The PWM rectifier can achieve good dynamic and steady-state performance with the help of hysteresis current controllers, which have simple control schemes as shown in Fig. 5. Reference current peak values are predicted using DC link voltage control, and accompanying unit vectors provide phase information. To ensure that the real current tracks the reference current, the hysteresis controller generates gating pulses at every switch. The DC voltage controller output current is multiplied by the amplitude of the three sinusoidal voltages. The mains voltage and these voltages are in perfect phase. At the neutral point, the voltage is balanced using a compensator. The power factor is corrected by tracking the line current with a hysteresis current controller.

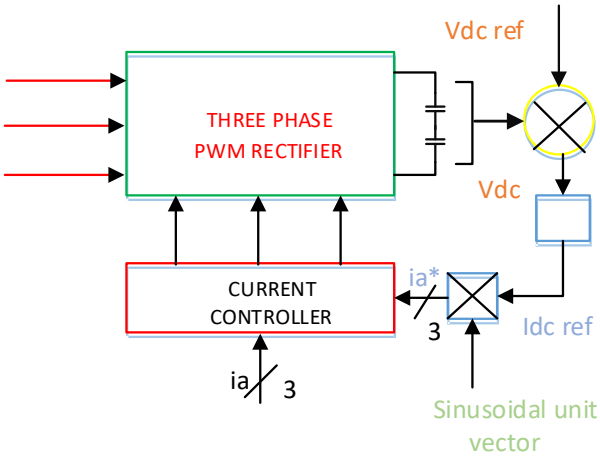

Fig 5. Control of Hysteresis Current in a PWM Rectifier

To achieve real-time feedback for current control in pulse width modulation (PWM), the hysteresis controller is used. The command current is monitored frequently within a preset hysteresis band to control the true current. The necessary reference current frequency and magnitude are generated by the control circuitry using a sinusoidal waveform. In this comparison, we look at the sinusoidal reference current waveform and compare it to the real phase current waveform. The hysteresis band is used to disable the switch when the sinusoidal reference current exceeds it. This causes a drop in current and an output voltage that swings between +0.5V and -0.5V. The switch is set to activate when the current surpasses the lower band limit. By turning the switch on and off in a periodic pattern, the sinusoidal reference wave is compelled to follow the current wave within the hysteresis zone.

7. Analysis of Simulation Results

It was built and tested to calculate the efficiency of a prototype based on a Vienna rectifier. The input voltage (Va, Vb, and Vc) for the three phases is 420V, and the frequency is 50 Hz as shown in Fig. 6, The desired values for the output voltage, current, and power are 810V, 19.45A, and 15.7 kW, are shown in Fig. 7. respectively. The inductance of the La, Lb, and Lc phase boost inductors is 0.3mH. The split DC-bus capacitors C1 and C2 have been chosen with an 8000 μF value. The MATLAB programme was enhanced to build a simulation model following Tab's design specifications and check the Vienna rectifier parameter design. The simulation outcomes were then looked at. It is obvious that the overshoot is reduced, the dynamic performance is better, and the stability can be quickly recovered. Table 3: The Vienna rectifier simulation model's primary parameters

Table 3. Vienna Rectifier Simulation Model Parameters

S.No	Symbol	Parameters	Value
1	V_{in}	Input voltage in volts	420V
2	F	Grid frequency in hertz	50hz
3	La, Lb, Lc	Inductor in mh	0.3H
4	C1, C2	capacitor in μf	7982000f
5	Vo	Output Voltage in volts	810V
6	Iout	Output current in Amps	19.45A
7	Pin	Input power	16Kw
8	η	Efficiency	98.12
9	Pout	Output Power in kW	15.7kW
10	fsw	Switching frequency	20khz
11	PF	Power factor	0.98

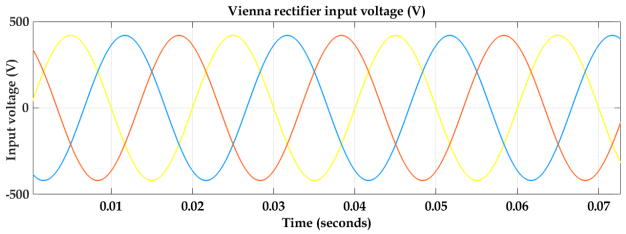

Fig. 6. Vienna rectifier input voltages.

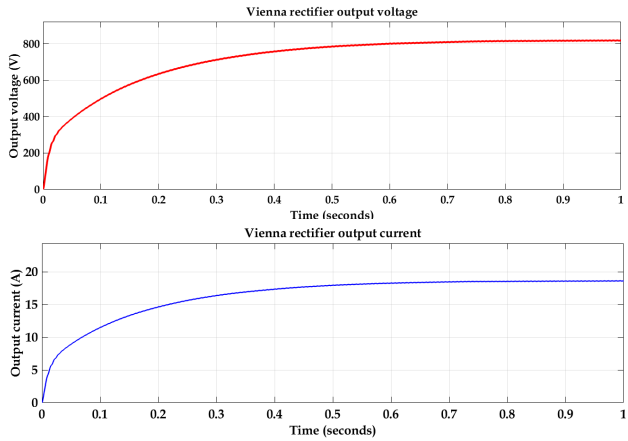

Fig. 7. shows the waveform of the output voltage and current.

Fig .8. shows the waveform that was utilized to determine total harmonic distortion. Low harmonics (3.43%) are to blame for the high distortion power factor, which in turn produces a massive power factor of 0.98.

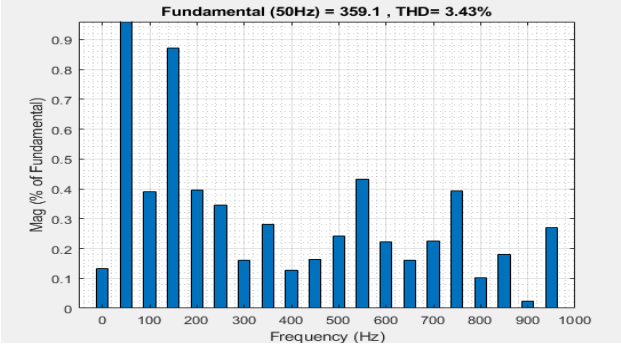

Fig. 8. THD percentage for the proposed Vienna Rectifier

8. Conclusion

This model represents a three-level, three-phase Vienna rectifier that uses voltage and current double-closed-loop control in its control algorithm. The voltage loop houses the PI controller, whereas the current loop houses the hysteresis controller. A three-phase Vienna rectifier is simulated and evaluated in this work using PI in conjunction with a hysteresis controller. Since they are unable to inherit zero steady-state error, hysteresis controllers outperform all others in terms of current control reactions, according to the simulation. Without changing the output voltage, the suggested current controllers in this study successfully enhanced waveform quality. In this study, a method for controlling and modulating the three-phase Vienna rectifier is proposed. Research into the rectifier concept, model construction, system design control, and simulation result validation comprise the study's methodology. This system satisfies the requirements of the IEEE-519 standard by keeping its power factor constant at unity and its overall distortion caused by harmonics in the input current below 5%. The Hysteresis current controller-based Vienna rectifier is a great option for electric vehicle charging stations due to its decreased total distortion caused by harmonics, significant power factor, and reduced necessary criteria for screening. The results of the simulations suggest that the new control strategy might lessen input side distortion caused by harmonics and enhance the dynamic properties of the DC side voltage.

References

[1] P. Maheshwari, Y. Tambawala, H. S. V. S. K. Nunna, and S. Doolla, "A review on plug-in electric vehicles charging: Standards and impact on distribution system," in *2014 IEEE Int. Conf. Pow. Electr., Driv. Ener. Sys,s (PEDES)*,Mumbai India: IEEE, Dec. 2014, pp. 1–6. doi: 10.1109/PEDES.2014.7042147.

[2] A. Pravin, "Standardization of protocol for charging Infrastructure," Ministry of Heavy Industries & Public Enterprises Department of Heavy Industry Govt. of India, 2017. [Online]. Available: https://heavyindustries.gov.in/sites/default/files/2023-09/Standardization%20of%20protocol.pdf

[3] A. Sharma and R. Gupta, "Bharat DC001 Charging standard Based EV Fast Charger," in *IECON 2020 The 46th Ann. Conf. IEEE Indust. Electron. Soc.*, Singapore, Singapore: IEEE, Oct. 2020, pp. 3588–3593. doi: 10.1109/IECON43393.2020.9254949.

[4] W. Khan, A. Ahmad, F. Ahmad, and M. Saad Alam, "A Comprehensive Review of Fast Charging Infrastructure for Electric Vehicles," *Smart Sci.*, vol. 6, no. 3, pp. 256–270, Mar. 2018, doi: 10.1080/23080477.2018.1437323.

[5] A. Khaligh and M. DAntonio, "Global Trends in High-Power On-Board Chargers for Electric Vehicles," *IEEE Trans. Veh. Technol.*, vol. 68, Art no. 4, Apr. 2019, doi: 10.1109/TVT.2019.2897050.

[6] Y. Du, S. Lukic, B. Jacobson, and A. Huang, "Review of high power isolated bi-directional DC-DC converters for PHEV/EV DC charging infrastructure," in *2011 IEEE Ener. Convers. Congr. Expos.*, Phoenix, AZ, USA: IEEE, Sep. 2011, pp. 553–560. doi: 10.1109/ECCE.2011.6063818.

[7] P. Vishnuram, S. P., N. R., V. K., and B. Nastasi, "Wireless Chargers for Electric Vehicle: A Systematic Review on Converter Topologies, Environmental Assessment, and Review Policy," *Energies*, vol. 16, no. 4., Art no. 1731, Feb. 2023. doi: 10.3390/en16041731.

[8] H. Tu, H. Feng, S. Srdic, and S. Lukic, "Extreme Fast Charging of Electric Vehicles: A Technology Overview," *IEEE Trans. Transp. Electrific.*, vol. 5, no. 4, pp. 861–878, Dec. 2019, doi: 10.1109/TTE.2019.2958709.

[9] M. Safayatullah, M. T. Elrais, S. Ghosh, R. Rezaii, and I. Batarseh, "A Comprehensive Review of Power Converter Topologies and Control Methods for Electric Vehicle Fast Charging Applications," *IEEE Access*, vol. 10, pp. 40753–40793, Apr. 2022, doi: 10.1109/ACCESS.2022.3166935.

[10] P. Vishnuram *et al.*, "A Comprehensive Review on EV Power Converter Topologies Charger Types Infrastructure and Communication Techniques," *Front. Energy Res.*, vol. 11, Feb. 2023, doi: 10.3389/fenrg.2023.1103093.

[11] M. R. Khalid, I. A. Khan, S. Hameed, M. S. J. Asghar, and J.-S. Ro, "A Comprehensive Review on Structural Topologies, Power Levels, Energy Storage Systems, and Standards for Electric Vehicle Charging Stations and Their Impacts on Grid," *IEEE Access*, vol. 9, pp. 128069–128094, Sep. 2021, doi: 10.1109/ACCESS.2021.3112189.

[12] T. B. Soeiro and J. W. Kolar, "Analysis of High-Efficiency Three-Phase Two- and Three-Level Unidirectional Hybrid Rectifiers," *IEEE Trans. Ind. Electron.*, vol. 60, no. 9, pp. 3589–3601, Sep. 2013, doi: 10.1109/TIE.2012.2205358.

[13] M. Zhang, L. Hang, W. Yao, Z. Lu, and L. M. Tolbert, "A Novel Strategy for Three-Phase/Switch/Level (Vienna) Rectifier Under Severe Unbalanced Grids," *IEEE Trans. Ind. Electron.*, vol. 60, no. 10, pp. 4243–4252, Apr. 2013, doi: 10.1109/TIE.2012.2217721.

[14] J. W. Kolar and F. C. Zach, "A novel three-phase utility interface minimizing line current harmonics of high-power telecommunications rectifier modules," *IEEE Trans. Ind. Electron.*, vol. 44, no. 4, pp. 456–467, Aug. 1997, doi: 10.1109/41.605619.

[15] A. Rajaei, M. Mohamadian, and A. Varjani, "Vienna-Rectifier-Based Direct Torque Control of PMSG for Wind Energy Application," *Ind. Electron. IEEE Trans.*, vol. 60, pp. 2919–2929, Jul. 2013, doi: 10.1109/TIE.2012.2227905.

[16] G. Rajendran, C. A. Vaithilingam, K. Naidu, and K. S. P. Oruganti, "Energy-efficient converters for electric vehicle charging stations," *SN Appl. Sci.*, vol. 2, no. 4, pp. 1–15, Mar. 2020, doi: 10.1007/s42452-020-2369-0.

[17] S. Panchanathan *et al.*, "A Comprehensive Review of the Bidirectional Converter Topologies for the Vehicle-to-Grid System," *Energies*, vol. 16, no. 5, Art. no. 2503, Mar. 2023, doi: 10.3390/en16052503.

[18] H. Cheng, W. Chen, C. Wang, and J. Deng, "Open Circuit Fault Diagnosis and Fault Tolerance of Three-Phase Bridgeless Rectifier," *Electronics*, vol. 7, no. 11. Art no. 291, Nov. 2018. doi: 10.3390/electronics7110291.

[19] J.-S. Lee and K.-B. Lee, "Open-Switch Fault Diagnosis and Tolerant Control Methods for a Vienna Rectifier Using Bi-Directional Switches," in *2018 IEEE Ener. Convers. Congr. Expos. (ECCE)*, Portland, OR, USA: IEEE, Sep. 2018, pp. 4129–4134. doi: 10.1109/ECCE.2018.8558280.

[20] Z. Junwei, Q. Yingning, F. Yanhui, and F. Kai, "Fault Tolerance for Wind Turbine Power Converter," in *2nd IET Renew. Power Generat. Conf. (RPG 2013)*, Beijing, China: Institution of Engineering and Technology, 2013, p. 3.24-3.24. doi: 10.1049/cp.2013.1831.

[21] J. Zou, C. Wang, H. Cheng, and J. Liu, "Triple Line-Voltage Cascaded VIENNA Converter Applied as the Medium-Voltage AC

Drive," *Energies*, vol. 11, no. 5., Art no. 1079, Apr. 2018. doi: 10.3390/en11051079.

[22] Y.D. Kwon, J.-H. Park, and K.-B. Lee, "Improving Line Current Distortion in Single-Phase Vienna Rectifiers Using Model-Based Predictive Control," *Energies*, vol. 11, no. 5., Art. no. 1237, May 2018. doi: 10.3390/en11051237.

[23] J. Chelladurai and B. Vinod, "Performance evaluation of three phase scalar controlled pwm rectifier using different carrier and modulating signal," *J. Eng. Sci. Technol.*, vol. 10, pp. 420–433, Apr. 2015.

[24] B. Kedjar, H. Y. Kanaan, and K. Al-haddad, "Vienna Rectifier With Power Quality Added Function," *IEEE Trans. Ind. Electron.*, vol. 61, pp. 3847–3856, Mar. 2014

[25] S. M. Cherati, N. A. Azli, S. M. Ayob, and A. Mortezaei, "Design of a current mode PI controller for a single-phase PWM inverter," in *2011 IEEE Appl. Pow. Electron. Colloquium (IAPEC)*, Johor Bahru, Malaysia: IEEE, Apr. 2011, pp. 180–184. doi: 10.1109/IAPEC.2011.5779864.

[26] G. Rajendran, C. A. Vaithilingam, N. Misron, K. Naidu, and M. R. Ahmed, "Voltage Oriented Controller Based Vienna Rectifier for Electric Vehicle Charging Stations," *IEEE Access*, vol. 9, pp. 50798–50809, Aug. 2021, doi: 10.1109/ACCESS.2021.3068653.

[27] E. M. Suhara and M. Nandakumar, "Analysis of hysteresis current control techniques for three phase PWM rectifiers," in *2015 IEEE Int. Conf. Sign. Process., Informat., Communic. Ener. Sys. (SPICES)*, Kozhikode, India: IEEE, Feb. 2015, pp. 1–5. doi: 10.1109/SPICES.2015.7091434.

[28] F. Wu, F. Feng, L. Luo, J. Duan, and L. Sun, "Sampling Period Online Adjusting-Based Hysteresis Current Control Without Band With Constant Switching Frequency," *Ind. Electron. IEEE Trans.*, vol. 62, pp. 270–277, Jan. 2015, doi: 10.1109/TIE.2014.2326992.

[29] M. Mohseni and S. Islam, "A New Vector-Based Hysteresis Current Control Scheme for Three-Phase PWM Voltage-Source Inverters," *Power Electron. IEEE Trans.*, vol. 25, pp. 2299–2309, Oct. 2010, doi: 10.1109/TPEL.2010.2047270.

[30] L. H. S. C. Barreto, J. B. Vieira, E. A. A. Coelho, V. J. Farias, and L. C. De Freitas, "The bang-bang hysteresis current waveshaping control technique used to implement a high power factor power supply," in *24th Ann. Int. Telecommun. Ener. Conf.*, Montreal, Que., Canada: IEEE, 2002, pp. 361–365. doi: 10.1109/INTLEC.2002.1048681.

[31] T. Yoshida, O. Shizuka, O. Miyashita, and K. Ohniwa, "An improvement technique for the efficiency of high-frequency switch-mode rectifiers," *IEEE Trans. Power Electron.*, vol. 15, no. 6, pp. 1118–1123, May 2000, doi: 10.1109/63.892826.

[32] T. M. Mohan, W. P. Undeland, O. Robbins, Joseph, and Suleman Aslam, "Power Electronics Converters Applications," *Cos. J. Phys.*, vol. 2, no. 1, pp. 1–40, Nov. 2023, doi: 10.13140/RG.2.2.36786.58562.

[33] M. H. Rashid, *Power electronics: circuits, devices, and applications*, 3rd ed. New Delhi: Dorling Kindersley, 2011.

[34] M. D. Singh and K. B. Khanchandani, *Power Electronics*, 2nd ed. New York: Tata McGraw-Hill, 2006.